Journal of Porous Media, 20(11):999–1016 (2017)

UNSTEADY FREE CONVECTION IN A SQUARE POROUS CAVITY SATURATED WITH NANOFLUID: THE CASE OF LOCAL THERMAL NONEQUILIBRIUM AND BUONGIORNO'S MATHEMATICAL MODELS

H. Zargartalebi,[1] M. Ghalambaz,[2] M.A. Sheremet,[3,4,] & I. Pop[5]*

[1]*Department of Mechanical Engineering, Shahid Chamran University of Ahvaz, Ahvaz, Iran*
[2]*Department of Mechanical Engineering, Dezful Branch, Islamic Azad University, Dezful, Iran*
[3]*Department of Theoretical Mechanics, Tomsk State University, 634050, Tomsk, Russia*
[4]*Institute of Power Engineering, Tomsk Polytechnic University, 634050, Tomsk, Russia*
[5]*Department of Applied Mathematics, Babeş-Bolyai University, 400084 Cluj-Napoca, Romania*

*Address all correspondence to: M.A. Sheremet, Tomsk State University, 36 Lenin Avenue, Tomsk, Russia, 634050, E-mail: Michael-sher@yandex.ru

Original Manuscript Submitted: 2/3/2016; Final Draft Received: 11/29/2016

Considering Buongiorno's model, the unsteady free convection in a porous enclosure filled with a nanofluid is studied while the nanoparticles, the base fluid, and the solid porous matrix are in local thermal nonequilibrium. It is assumed that the left and right vertical walls are suddenly heated and cooled. Moreover, the movement of the nanoparticles is affected by Brownian and thermophoresis forces. The influence of multifarious thermophysical variables, such as solid–fluid and nanoparticle–fluid interaction heat transfer parameters, buoyancy ratio parameter, and Rayleigh number, on the transient average Nusselt number for the solid matrix, the base fluid, and the nanoparticles is investigated. It is found that the increase of solid–fluid and nanoparticle–fluid interaction heat transfer parameters would majorly augment the solid and nanoparticle average Nusselt numbers, respectively. Furthermore, the decrease of the buoyancy ratio and the increase of Rayleigh number would boost the average Nusselt number for all of the three phases. Eventually, the period of reaching to steady state shows a direct proportion to buoyancy ratio and a reverse proportion to Rayleigh number.

KEY WORDS: *unsteady free convection, porous media, thermal nonequilibrium model, nanofluids, Buongiorno's model*

1. INTRODUCTION

Convective heat transfer of nanofluid-saturated porous media has attracted considerable attention due to wide applications in engineering, such as electronic geothermal systems, chemical catalytic reactors, component cooling, packed sphere beds, and paper production. Porous structures are also enthusiastic in relation to solar power collectors and the underground spread of pollutants. In fact, the mechanical systems due to external power supply almost are doomed to failure, and therefore a reliable natural convection system could be an appropriate alternative to mechanical systems. It also substantially declines the induced noise because of the fans. Accordingly, because of such virtues, many engineers and investigators are fascinated by natural convection phenomena. There is a rich literature concerning the convective flows in porous media, such as Nield and Bejan (2013), Ingham and Pop (2005), Vafai (2005, 2010), Bejan and Kraus (2003), Narasimhan (2013), Bejan (2013), and Shenoy et al. (2016).

In essence, when the thermal conductivity of the porous structure is relatively low or the interaction between porous medium and fluid is high, perfectly rational is the assumption that the temperatures of porous medium and

1091–028X/17/$35.00

NOMENCLATURE

C	nanoparticle volume fraction
C_0	ambient nanoparticle volume fraction
D_B	Brownian diffusion coefficient
D_T	thermophoretic diffusion coefficient
g	gravitational acceleration vector
h_{fp}	interface heat transfer coefficient between the fluid/particle phases
h_{fs}	interface heat transfer coefficient between the fluid/solid-matrix phases
K	permeability of the porous medium
k	effective thermal conductivity
L	cavity size
Le	Lewis number
N	total number of nodes
Nb	Brownian motion parameter
Nhp	Nield number for the fluid/nanoparticle interface (fluid/nanoparticle interface parameter)
Nhs	Nield number for the fluid/solid-matrix interface (fluid/solid-matrix interface parameter)
Nr	buoyancy ratio parameter
Nt	thermophoresis parameter
Nu	local Nusselt number
$\overline{\text{Nu}}$	average Nusselt number
p	pressure
R	residual of weak form
Ra	thermal Rayleigh–Darcy number $\text{Ra} = (1 - C_0)\, gK\rho_{f0}\beta\Delta TL/(\alpha_f \mu)$
Sh	local Sherwood number
$\overline{\text{Sh}}$	average Sherwood number
T	nanofluid temperature
T_c	temperature at the right wall
T_h	temperature at the left wall
$\bar{u}, \bar{v}$	the velocity components along $\bar{x}$, $\bar{y}$ directions
V	Darcy velocity
$\bar{x}$, $\bar{y}$	Cartesian coordinates

Greek Symbols

α	effective thermal diffusivity
β	thermal expansion coefficient
γ_p	modified particle heat capacity
γ_s	modified porous solid matrix thermal conductivity
ε	porosity
ε_p	modified diffusivity ratio boundary
Θ	nondimensional temperature
μ	dynamic viscosity
ρ	fluid density
(ρc)	effective heat capacity
η	parameter defined by $\eta = (\rho c)_p/(\rho c)_f$
ξ	basis functions
τ	dimensionless time
φ	relative nanoparticle volume fraction
ψ	nondimensional stream function
$\bar{\psi}$	stream function

Subscripts

0	the ambient property
f	base fluid phase
i	residual number
k	node number
p	nanoparticle phase
s	porous medium solid-matrix phase

fluid are much the same and the mixture is in local thermal equilibrium (LTE). This consideration facilitates the problem so that the fluid and porous structure can be assumed as a uniform mixture. Nevertheless, in several other cases, there are substantial temperature differences between the fluid and the porous medium. In such cases, the assumption of LTE is no longer valid and the local thermal nonequilibrium between the porous matrix and the fluid is much better considered (see Ingham and Pop, 2005; Baytas and Pop, 2002; Baytas, 2003; Jamalabadi, 2015; Wu and Zhou, 2016).

To modify the specifications of the fluid, investigators have manufactured an engineered fluid in which some particles in size of nanometer are mixed with a base fluid, called nanofluid. Several investigations have been established to evaluate the characteristics and heat transfer of multifarious kinds of nanofluids (see Zhang et al., 2008; Hirota et al., 2010; Choi et al., 2008; Khanafer and Vafai, 2011; Gümgüm and Tezer-Sezgin, 2014; Mahajan and

Sharma, 2014). Buongiorno (2006) examined the nanoparticle mass transfer in nanofluids utilizing scale analysis and found that the thermophoresis and Brownian motion are two significant particle transfer mechanisms in nanofluid. The thermophoresis force induces the force, which tends to move the nanoparticles based on temperature gradient (nanoparticles move from the hot side to the cold side), and the Brownian motion force makes uniform nanoparticles in the fluid.

Nanoscience is an interdisciplinary field of science which has its early beginnings in the 1980s. At small dimensions of a few nanometers (billionths of a meter), new physical properties emerge, often due to quantum mechanical effects. During the last decades, additionally, novel microscopical techniques have been developed to observe, measure, and manipulate objects at the nanoscale. It rapidly turned out that nanosized features not only play a role in physics and materials sciences but also are most relevant in chemistry, biology, and medicine, giving rise to new fenestrations between these disciplines and wide application prospects (see Schaefer, 2009). Therefore nanofluid technology, a new interdisciplinary field of great importance, where nanoscience, nanotechnology, and thermal engineering meet, has been largely developed over the past three decades.

The unsteady free convection of a regular flow in a cavity implementing local thermal equilibrium has been investigated by previous researchers. For instance, Saeid and Pop (2004), considering an enclosure in which the left vertical wall was suddenly heated to a constant high temperature and the right vertical wall was cooled suddenly to a constant low temperature, calculated the local and average Nusselt numbers for different Rayleigh numbers. Muthtamilselvan (2011), taking into account the left vertical wall in three different partially heated locations, studied the transient buoyancy-driven convection in a water-saturated porous enclosure near its density maximum. In a series of investigations, spearheaded by Amiri and Vafai (1994, 1998) and Vafai and Amiri (1998), the substantiation of the LTE assumption and its domain of applicability have been discussed.

On the other hand, several studies have been conducted to analyze the free convection in an enclosure of a saturated porous medium using a local thermal nonequilibrium model. For example, Khashan et al. (2006) examined the numerical simulation of the natural convection heat transfer in a porous cavity incorporating different non-Darcian effects, such as Brinkman, Forchhiemer quadratic inertial, and the convective terms. Srivastava et al. (2011), using the Darcy model with anisotropic permeability, analyzed the onset of thermal convection in an electrically conducting fluid-saturated porous medium, when the fluid and solid phases are not in LTE. Jaballah et al. (2012) numerically investigated the nonequilibrium thermal transfer of heat occurring between the coolant fluid and the exchanger (channel) partially filled by successive porous matrices.

The motivation behind the present work is to study the unsteady free convection in a porous enclosure saturated by nanofluid in which the local thermal nonequilibrium and Buongiorno's model are considered. The effect of different thermophysical variables, such as solid–fluid and nanoparticle–fluid interaction heat transfer parameters, buoyancy ratio parameter, Nhs, and Nhp on transient average Nusselt number is investigated. It is worth mentioning to this end that after Telionis (1981), there is no actual flow situation, natural or artificial, that does not involve some unsteadiness. For a long time, the flow in all engineering applications was arbitrarily assumed to be steady. For example, the lifting characteristics of an airfoil or the drag characteristics of a blunt body were problems attacked both analytically and experimentally as steady problems. It is well known, however, that in many other engineering applications, unsteadiness is an integral part of the problem.

2. MATHEMATICAL FORMULATION

A two-dimensional unsteady free convection in an enclosure filled with a porous matrix and saturated with a nanofluid is considered. It is assumed that the three phases, namely, porous structure, base fluid, and nanoparticles, are not in thermal equilibrium. In addition, the nanoparticles are suspended in the nanofluid utilizing surface charge technology or surfactant. Indeed, this averts the nanoparticles from agglomeration on the porous matrix or agglutination together (see Kuznetsov and Nield, 2010, 2013; Nield and Kuznetsov, 2009, 2014). A schematic of the physical model is presented in Fig. 1.

It is presumed that the left vertical wall is suddenly heated to T_h and the right vertical wall is suddenly cooled to T_c, where $T_h > T_c$. The bottom and top horizontal walls are insulated. The enclosure walls are considered to be rigid,

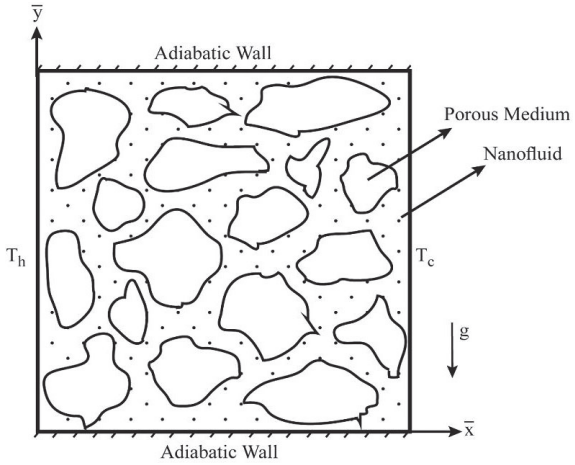

FIG. 1: Schematic of coordinate system and physical model

nonconducting, and impermeable. Moreover, the porous matrix is assumed to be isotropic and homogenous throughout the enclosure. Apart from density variation in the buoyancy force, which conformed to Boussinesq approximation, the other physical properties of the nanofluid and porous medium are considered to be constant.

The unsteady form of the governing equations for mass, momentum, and thermal energy in the fluid phase, particle phase, and solid-matrix phase and the conservation for nanoparticles are represented here in canonical form as derived by several researchers (see Khanafer and Vafai, 2011; Khashan et al., 2006; Kuznetsov and Nield, 2010; Nield and Kuznetsov, 2009, 2014; Tzou, 2008a,b):

$$\nabla \cdot \mathbf{V} = 0 \tag{1}$$

$$\frac{\mu}{K}\mathbf{V} = -\nabla p + \left[C\rho_p + (1-C)\,\rho_{f0}\,(1-\beta\,(T_f - T_c))\right]\mathbf{g} \tag{2}$$

$$\frac{\partial T_f}{\partial t} + \frac{1}{\varepsilon}\mathbf{V}\cdot\nabla T_f = \frac{k_f}{(\rho c)_f}\nabla^2 T_f + \tau\left(D_B \nabla C\cdot\nabla T_f + \frac{D_T}{T_c}\nabla T_f\cdot\nabla T_f\right) + \frac{[h_{fp}\,(T_p - T_f) + h_{fs}\,(T_s - T_f)]}{\varepsilon\,(1-C_0)\,(\rho\,c)_f} \tag{3}$$

$$\frac{\partial T_p}{\partial t} + \frac{1}{\varepsilon}\mathbf{V}\cdot\nabla T_p = \frac{k_p}{(\rho c)_p}\nabla^2 T_p + \frac{h_{fp}}{\varepsilon C_0\,(\rho c)_p}\,(T_f - T_p) \tag{4}$$

$$\frac{\partial T_s}{\partial t} = \frac{k_s}{(\rho c)_s}\nabla^2 T_s + \frac{h_{fs}}{(1-\varepsilon)\,(\rho c)_s}\,(T_f - T_s) \tag{5}$$

$$\frac{\partial C}{\partial t} + \frac{1}{\varepsilon}\mathbf{V}\cdot\nabla C = D_B\nabla^2 C + \frac{D_T}{T_c}\,\nabla^2 T_f \tag{6}$$

Equations (1)–(6) for the problem under consideration can be written in dimensional Cartesian coordinates $\bar{x}$, $\bar{y}$ taking into account the slow flow and dilute nanoparticle concentration, as follows:

$$\frac{\partial \bar{u}}{\partial \bar{x}} + \frac{\partial \bar{v}}{\partial \bar{y}} = 0 \tag{7}$$

$$\frac{\partial p}{\partial \bar{x}} = -\frac{\mu}{K}\bar{u} \tag{8}$$

$$\frac{\partial p}{\partial \bar{y}} = -\frac{\mu}{K}\bar{v} - [C\,(\rho_p - \rho_{f0}) + \rho_{f0}\,(1 - \beta\,(T_f - T_c)\,(1-C_0))]\;g \tag{9}$$

$$\frac{\partial T_f}{\partial t}+\frac{1}{\varepsilon}\left(\bar{u}\frac{\partial T_f}{\partial \bar{x}}+\bar{v}\frac{\partial T_f}{\partial \bar{y}}\right)=\alpha_f\left(\frac{\partial^2 T_f}{\partial \bar{x}^2}+\frac{\partial^2 T_f}{\partial \bar{y}^2}\right)+\eta\left\{D_B\left(\frac{\partial C}{\partial \bar{x}}\frac{\partial T_f}{\partial \bar{x}}+\frac{\partial C}{\partial \bar{y}}\frac{\partial T_f}{\partial \bar{y}}\right)+\left(\frac{D_T}{T_c}\right)\left[\left(\frac{\partial T_f}{\partial \bar{x}}\right)^2+\left(\frac{\partial T_f}{\partial \bar{y}}\right)^2\right]\right\}+\frac{\left[h_{fp}\left(T_p-T_f\right)+h_{fs}\left(T_s-T_f\right)\right]}{\varepsilon\left(1-C_0\right)\left(\rho\, c\right)_f} \tag{10}$$

$$\frac{\partial T_p}{\partial t}+\frac{1}{\varepsilon}\left(\bar{u}\frac{\partial T_p}{\partial \bar{x}}+\bar{v}\frac{\partial T_p}{\partial \bar{y}}\right)=\alpha_p\left(\frac{\partial^2 T_p}{\partial \bar{x}^2}+\frac{\partial^2 T_p}{\partial \bar{y}^2}\right)+\frac{h_{fp}}{\varepsilon C_0\left(\rho c\right)_p}\left(T_f-T_p\right) \tag{11}$$

$$\frac{\partial T_s}{\partial t}=\alpha_s\left(\frac{\partial^2 T_s}{\partial \bar{x}^2}+\frac{\partial^2 T_s}{\partial \bar{y}^2}\right)+\frac{h_{fs}}{\left(1-\varepsilon\right)\left(\rho c\right)_s}\left(T_f-T_s\right) \tag{12}$$

$$\frac{\partial C}{\partial t}+\frac{1}{\varepsilon}\left(\bar{u}\frac{\partial C}{\partial \bar{x}}+\bar{v}\frac{\partial C}{\partial \bar{y}}\right)=D_B\left(\frac{\partial^2 C}{\partial \bar{x}^2}+\frac{\partial^2 C}{\partial \bar{y}^2}\right)+\left(\frac{D_T}{T_c}\right)\left(\frac{\partial^2 T_f}{\partial \bar{x}^2}+\frac{\partial^2 T_f}{\partial \bar{y}^2}\right) \tag{13}$$

Here $\bar{u}$, $\bar{v}$ are the velocity components along the $\bar{x}$, $\bar{y}$ axes, respectively. T_f, T_p, and T_s are the fluid, particle, and solid matrix temperatures, respectively. The physical meanings of the other quantities are mentioned in the nomenclature.

Introducing a stream function $\bar{\psi}$, defined as $\bar{u}=(\partial\bar{\psi})/(\partial\bar{y})$, $\bar{v}=-(\partial\bar{\psi})/(\partial\bar{x})$, Eq. (7) is satisfied identically. We are then left with the following equations:

$$\frac{\partial^2\bar{\psi}}{\partial\bar{x}^2}+\frac{\partial^2\bar{\psi}}{\partial\bar{y}^2}=-\frac{\left(1-C_0\right)\rho_{f0}gK\beta}{\mu}\frac{\partial T_f}{\partial\bar{x}}+\frac{\rho_p-\rho_{f0}}{\mu}gK\frac{\partial C}{\partial\bar{x}} \tag{14}$$

$$\frac{\partial T_f}{\partial t}+\frac{1}{\varepsilon}\left(\frac{\partial\bar{\psi}}{\partial\bar{y}}\frac{\partial T_f}{\partial\bar{x}}-\frac{\partial\bar{\psi}}{\partial\bar{x}}\frac{\partial T_f}{\partial\bar{y}}\right)=\alpha_f\left(\frac{\partial^2 T_f}{\partial\bar{x}^2}+\frac{\partial^2 T_f}{\partial\bar{y}^2}\right)+\eta\left\{D_B\left(\frac{\partial C}{\partial\bar{x}}\frac{\partial T_f}{\partial\bar{x}}+\frac{\partial C}{\partial\bar{y}}\frac{\partial T_f}{\partial\bar{y}}\right)+\left(\frac{D_T}{T_c}\right)\left[\left(\frac{\partial T_f}{\partial\bar{x}}\right)^2+\left(\frac{\partial T_f}{\partial\bar{y}}\right)^2\right]\right\}+\frac{\left[h_{fp}\left(T_p-T_f\right)+h_{fs}\left(T_s-T_f\right)\right]}{\varepsilon\left(1-C_0\right)\left(\rho\, c\right)_f} \tag{15}$$

$$\frac{\partial T_p}{\partial t}+\frac{1}{\varepsilon}\left(\frac{\partial\bar{\psi}}{\partial\bar{y}}\frac{\partial T_p}{\partial\bar{x}}-\frac{\partial\bar{\psi}}{\partial\bar{x}}\frac{\partial T_p}{\partial\bar{y}}\right)=\alpha_p\left(\frac{\partial^2 T_p}{\partial\bar{x}^2}+\frac{\partial^2 T_p}{\partial\bar{y}^2}\right)+\frac{h_{fp}}{\varepsilon C_0\left(\rho c\right)_p}\left(T_f-T_p\right) \tag{16}$$

$$\frac{\partial T_s}{\partial t}=\alpha_s\left(\frac{\partial^2 T_s}{\partial\bar{x}^2}+\frac{\partial^2 T_s}{\partial\bar{y}^2}\right)+\frac{h_{fs}}{\left(1-\varepsilon\right)\left(\rho c\right)_s}\left(T_f-T_s\right) \tag{17}$$

$$\frac{\partial C}{\partial t}+\frac{1}{\varepsilon}\left(\frac{\partial\bar{\psi}}{\partial\bar{y}}\frac{\partial C}{\partial\bar{x}}-\frac{\partial\bar{\psi}}{\partial\bar{x}}\frac{\partial C}{\partial\bar{y}}\right)=D_B\left(\frac{\partial^2 C}{\partial\bar{x}^2}+\frac{\partial^2 C}{\partial\bar{y}^2}\right)+\left(\frac{D_T}{T_c}\right)\left(\frac{\partial^2 T_f}{\partial\bar{x}^2}+\frac{\partial^2 T_f}{\partial\bar{y}^2}\right) \tag{18}$$

It is convenient to cast the conservation equations onto terms of dimensionless variables, such as

$$\begin{gathered}x=\bar{x}/L,\quad y=\bar{y}/L,\quad \psi=\bar{\psi}/\alpha_f,\quad \varphi=C/C_0,\quad \tau=\alpha_f t/\varepsilon L^2\\ \theta_f=(T_f-T_c)/\Delta T,\quad \theta_p=(T_p-T_c)/\Delta T,\quad \theta_s=(T_s-T_c)/\Delta T\end{gathered} \tag{19}$$

where $\Delta T=T_h-T_c$, and substituting Eq. (19) into Eqs. (14)–(18), we obtain

$$\frac{\partial^2\psi}{\partial x^2}+\frac{\partial^2\psi}{\partial y^2}=-\mathrm{Ra}\frac{\partial\theta_f}{\partial x}+\mathrm{Ra}\cdot Nr\frac{\partial\varphi}{\partial x} \tag{20}$$

$$\frac{\partial\theta_f}{\partial\tau}+\frac{\partial\psi}{\partial y}\frac{\partial\theta_f}{\partial x}-\frac{\partial\psi}{\partial x}\frac{\partial\theta_f}{\partial y}=\varepsilon\left(\frac{\partial^2\theta_f}{\partial x^2}+\frac{\partial^2\theta_f}{\partial y^2}\right)+Nb\left(\frac{\partial\phi}{\partial x}\frac{\partial\theta_f}{\partial x}+\frac{\partial\phi}{\partial y}\frac{\partial\theta_f}{\partial y}\right)+Nt\left[\left(\frac{\partial\theta_f}{\partial x}\right)^2+\left(\frac{\partial\theta_f}{\partial y}\right)^2\right]+Nhp\left(\theta_p-\theta_f\right)+Nhs\left(\theta_s-\theta_f\right) \tag{21}$$

$$\frac{\partial\theta_p}{\partial\tau}+\frac{\partial\psi}{\partial y}\frac{\partial\theta_p}{\partial x}-\frac{\partial\psi}{\partial x}\frac{\partial\theta_p}{\partial y}=\varepsilon_p\left(\frac{\partial^2\theta_p}{\partial x^2}+\frac{\partial^2\theta_p}{\partial y^2}\right)+Nhp\cdot\gamma_p\left(\theta_f-\theta_p\right) \tag{22}$$

$$\frac{\partial \theta_s}{\partial \tau} = \varepsilon \left(\frac{\partial^2 \theta_s}{\partial x^2} + \frac{\partial^2 \theta_s}{\partial y^2} \right) + Nhs \cdot \gamma_s \left(\theta_f - \theta_s \right) \tag{23}$$

$$\frac{\partial \varphi}{\partial \tau} + \frac{\partial \psi}{\partial y}\frac{\partial \varphi}{\partial x} - \frac{\partial \psi}{\partial x}\frac{\partial \varphi}{\partial y} = \frac{1}{\mathrm{Le}} \left(\frac{\partial^2 \varphi}{\partial x^2} + \frac{\partial^2 \varphi}{\partial y^2} \right) + \frac{Nt}{\mathrm{Le} \cdot Nb} \left(\frac{\partial^2 \theta_f}{\partial x^2} + \frac{\partial^2 \theta_f}{\partial y^2} \right) \tag{24}$$

The preceding equations are subjected to the following initial and boundary conditions (see also Kuznetsov and Nield, 2013):

$$\begin{aligned}
&\psi(x,y,0) = 0, \quad \theta_f(x,y,0) = \theta_p(x,y,0) = \theta_s(x,y,0) = 0.5, \quad \varphi(x,y,0) = 1 \\
&\psi(0,y,\tau) = 0, \quad \theta_f(0,y,\tau) = \theta_p(0,y,\tau) = \theta_s(0,y,\tau) = 1, \quad Nb\frac{\partial \varphi(0,y,\tau)}{\partial x} + Nt\frac{\partial \theta_f(0,y,\tau)}{\partial x} = 0 \\
&\psi(1,y,\tau) = 0, \quad \theta_f(1,y,\tau) = \theta_p(1,y,\tau) = \theta_s(1,y,\tau) = 0, \quad Nb\frac{\partial \varphi(1,y,\tau)}{\partial x} + Nt\frac{\partial \theta_f(1,y,\tau)}{\partial x} = 0 \\
&\psi(x,0,\tau) = 0, \quad \frac{\partial \theta_f(x,0,\tau)}{\partial y} = \frac{\partial \theta_p(x,0,\tau)}{\partial y} = \frac{\partial \theta_s(x,0,\tau)}{\partial y} = 0, \quad \frac{\partial \varphi(x,0,\tau)}{\partial y} = 0 \\
&\psi(x,1,\tau) = 0, \quad \frac{\partial \theta_f(x,1,\tau)}{\partial y} = \frac{\partial \theta_p(x,1,\tau)}{\partial y} = \frac{\partial \theta_s(x,1,\tau)}{\partial y} = 0, \quad \frac{\partial \varphi(x,1,\tau)}{\partial y} = 0
\end{aligned} \tag{25}$$

Here the nine parameters Nr, Nb, Nt, Nhp, Nhs, ε_p, γ_p, γ_s, and Le denote a buoyancy ratio parameter, a Brownian motion parameter, a thermophoresis parameter, the interface heat transfer parameters called Nield numbers (see Vadász, 2008), a modified thermal diffusivity ratio, modified thermal capacity ratios, and Lewis number, respectively, which are described as

$$\begin{aligned}
&Nr = \frac{(\rho_p - \rho_{f0})C_0}{\rho_{f0}\beta\Delta T(1-C_0)}, \quad Nb = \frac{\tau D_B C_0 \varepsilon}{\alpha_f}, \quad Nt = \frac{\tau D_T \varepsilon \Delta T}{\alpha_f T_c}, \quad Nhp = \frac{h_{fp}L^2}{k_f(1-C_0)}, \\
&Nhs = \frac{h_{fs}L^2}{k_f(1-C_0)}, \quad \varepsilon_p = \frac{\alpha_p \varepsilon}{\alpha_f}, \quad \gamma_p = \frac{(1-C_0)(\rho c)_f}{C_0(\rho c)_p}, \quad \gamma_s = \frac{k_f \varepsilon(1-C_0)}{k_s(1-\varepsilon)}, \quad \mathrm{Le} = \frac{\alpha_f}{D_B \varepsilon}
\end{aligned} \tag{26}$$

The interesting physical quantities are the local Nusselt numbers Nu_f, Nu_p, and Nu_s; the local Sherwood number Sh; the average Nusselt numbers $\overline{\mathrm{Nu}_f}$, $\overline{\mathrm{Nu}_p}$, $\overline{\mathrm{Nu}_s}$; and Sherwood number $\overline{\mathrm{Sh}}$.

Therefore the local Nusselt and Sherwood numbers are defined as follows:

$$\mathrm{Nu}_f = -\left(\frac{\partial \theta_f}{\partial x} \right)_{x=0}, \quad \mathrm{Nu}_p = -\left(\frac{\partial \theta_p}{\partial x} \right)_{x=0}, \quad \mathrm{Nu}_s = -\left(\frac{\partial \theta_s}{\partial x} \right)_{x=0}, \quad \mathrm{Sh} = -\left(\frac{\partial \varphi}{\partial x} \right)_{x=0} \tag{27}$$

The average Nusselt and Sherwood numbers are defined as

$$\overline{\mathrm{Nu}_f} = \int_0^1 \mathrm{Nu}_f \, dy, \quad \overline{\mathrm{Nu}_p} = \int_0^1 \mathrm{Nu}_p \, dy, \quad \overline{\mathrm{Nu}_s} = \int_0^1 \mathrm{Nu}_s \, dy, \quad \overline{\mathrm{Sh}} = \int_0^1 \mathrm{Sh} \, dy \tag{28}$$

It should be noticed here that for analyzing of Sherwood numbers, it is viable to investigate only Nusselt numbers because at the left and right vertical walls, we have $(\partial\varphi)/(\partial x) = -(Nt/Nb)[\partial\theta_f/\partial x]$, considering boundary conditions for φ [Eq. (25)]. Hence the additional examination regarding integral parameters will be only average Nusselt number owing to $\mathrm{Sh} = -(Nt/Nb)\mathrm{Nu}_f$ and $\overline{\mathrm{Sh}} = -(Nt/Nb)\overline{\mathrm{Nu}_f}$.

3. METHOD OF SOLUTION AND VALIDATION

Employing different kinds of finite element methods to solve industrial and environmental fluid mechanics problems is of interest recently (see Li and An, 2015; Solin et al., 2010). Therefore the system of partial differential

equations (20)–(24) along with the boundary conditions of Eq. (25) were transformed to weak form and solved numerically utilizing the Galerkin finite element method (see Reddy, 1993). The stream function (ψ), concentration of nanoparticles (φ), and the temperature of three phases (θ_f, θ_s, and θ_p) could be expanded utilizing basis set $\{\xi_k\}_{k=1}^{N}$ as

$$\begin{aligned}
&\psi \approx \sum_{k=1}^{N} \psi_k \xi_k(x,y), \;\; \varphi \approx \sum_{k=1}^{N} \varphi_k \xi_k(x,y), \;\; \theta_f \approx \sum_{k=1}^{N} \theta_{f_k} \xi_k(x,y), \\
&\theta_s \approx \sum_{k=1}^{N} \theta_{s_k} \xi_k(x,y), \;\; \theta_p \approx \sum_{k=1}^{N} \theta_{p_k} \xi_k(x,y)
\end{aligned} \tag{29}$$

for $-0.5 < x < 0.5$ and $0 < y < 1$. The basis functions for all five variables are the same. Hence the total number of nodes for all of them is N. Using the Galerkin finite element method, the ensuing nonlinear residual equations for Eqs. (20)–(24), respectively, at nodes of internal domain Ω are derived as

$$\begin{aligned}
R_i^1 = &\sum_{k=1}^{N} \psi_k \int_\Omega \left[\frac{\partial \xi_i}{\partial x}\frac{\partial \xi_k}{\partial x} + \frac{\partial \xi_i}{\partial y}\frac{\partial \xi_k}{\partial y} \right] dxdy - \int_\Gamma \xi_i n.\nabla\psi d\Gamma - \mathrm{Ra}\left(\sum_{k=1}^{N} \theta_{f_k} \int_\Omega \frac{\partial \xi_k}{\partial x} \xi_i dxdy \right) \\
&+ \mathrm{Ra} \cdot Nr \left(\sum_{k=1}^{N} \varphi \int_\Omega \frac{\partial \xi_k}{\partial x} \xi_i dxdy \right)
\end{aligned} \tag{30}$$

$$\begin{aligned}
R_i^2 = &\sum_{k=1}^{N} \theta_{f_k} \int_\Omega \frac{\partial \xi_k}{\partial \tau} \xi_i dxdy + \left(\sum_{k=1}^{N} \psi_k \int_\Omega \frac{\partial \xi_k}{\partial y} \xi_i dxdy \right) \left(\sum_{k=1}^{N} \theta_{f_k} \int_\Omega \frac{\partial \xi_k}{\partial x} \xi_i dxdy \right) \\
&- \left(\sum_{k=1}^{N} \psi_k \int_\Omega \frac{\partial \xi_k}{\partial x} \xi_i dxdy \right) \left(\sum_{k=1}^{N} \theta_{f_k} \int_\Omega \frac{\partial \xi_k}{\partial y} \xi_i dxdy \right) + \varepsilon \left[\sum_{k=1}^{N} \theta_{f_k} \int_\Omega \left(\frac{\partial \xi_i}{\partial x}\frac{\partial \xi_k}{\partial x} + \frac{\partial \xi_i}{\partial y}\frac{\partial \xi_k}{\partial y} \right) \right] \\
&+ Nb \left[\left(\sum_{k=1}^{N} \varphi_k \int_\Omega \frac{\partial \xi_k}{\partial x} \xi_i dxdy \right) \left(\sum_{k=1}^{N} \theta_{f_k} \int_\Omega \frac{\partial \xi_k}{\partial x} \xi_i dxdy \right) + \left(\sum_{k=1}^{N} \varphi_k \int_\Omega \frac{\partial \xi_k}{\partial y} \xi_i dxdy \right) \right. \\
&\left. \times \left(\sum_{k=1}^{N} \theta_{f_k} \int_\Omega \frac{\partial \xi_k}{\partial y} \xi_i dxdy \right) \right] + Nt \left[\left(\sum_{k=1}^{N} \theta_{f_k} \int_\Omega \frac{\partial \xi_k}{\partial x} \xi_i dxdy \right)^2 + \left(\sum_{k=1}^{N} \theta_{f_k} \int_\Omega \frac{\partial \xi_k}{\partial y} \xi_i dxdy \right)^2 \right] \\
&- Nhp \left[\int_\Omega \left(\sum_{k=1}^{N} \theta_{p_k} \xi_k - \sum_{k=1}^{N} \theta_{f_k} \xi_k \right) \xi_i dxdy \right] - Nhs \left[\int_\Omega \left(\sum_{k=1}^{N} \theta_{s_k} \xi_k - \sum_{k=1}^{N} \theta_{f_k} \xi_k \right) \xi_i dxdy \right]
\end{aligned} \tag{31}$$

$$\begin{aligned}
R_i^3 = &\sum_{k=1}^{N} \theta_{p_k} \int_\Omega \frac{\partial \xi_k}{\partial \tau} \xi_i dxdy + \left(\sum_{k=1}^{N} \psi_k \int_\Omega \frac{\partial \xi_k}{\partial y} \xi_i dxdy \right) \left(\sum_{k=1}^{N} \theta_{p_k} \int_\Omega \frac{\partial \xi_k}{\partial x} \xi_i dxdy \right) \\
&- \left(\sum_{k=1}^{N} \psi_k \int_\Omega \frac{\partial \xi_k}{\partial x} \xi_i dxdy \right) \left(\sum_{k=1}^{N} \theta_{p_k} \int_\Omega \frac{\partial \xi_k}{\partial y} \xi_i dxdy \right) + \varepsilon_p \left[\sum_{k=1}^{N} \theta_{p_k} \int_\Omega \left(\frac{\partial \xi_i}{\partial x}\frac{\partial \xi_k}{\partial x} + \frac{\partial \xi_i}{\partial y}\frac{\partial \xi_k}{\partial y} \right) \right] \\
&- Nhp \cdot \gamma_p \left[\int_\Omega \left(\sum_{k=1}^{N} \theta_{f_k} \xi_k - \sum_{k=1}^{N} \theta_{p_k} \xi_k \right) \xi_i dxdy \right]
\end{aligned} \tag{32}$$

$$\begin{aligned}
R_i^4 = &\sum_{k=1}^{N} \theta_{s_k} \int_\Omega \frac{\partial \xi_k}{\partial \tau} \xi_i dxdy + \varepsilon \left[\sum_{k=1}^{N} \theta_{s_k} \int_\Omega \left(\frac{\partial \xi_i}{\partial x}\frac{\partial \xi_k}{\partial x} + \frac{\partial \xi_i}{\partial y}\frac{\partial \xi_k}{\partial y} \right) \right] \\
&- Nhs \cdot \gamma_s \left[\int_\Omega \left(\sum_{k=1}^{N} \theta_{f_k} \xi_k - \sum_{k=1}^{N} \theta_{s_k} \xi_k \right) \xi_i dxdy \right]
\end{aligned} \tag{33}$$

$$R_i^5 = \sum_{k=1}^{N} \varphi_k \int_\Omega \frac{\partial \xi_k}{\partial \tau} \xi_i dxdy + \left(\sum_{k=1}^{N} \psi_k \int_\Omega \frac{\partial \xi_k}{\partial y} \xi_i dxdy \right) \left(\sum_{k=1}^{N} \varphi_k \int_\Omega \frac{\partial \xi_k}{\partial x} \xi_i dxdy \right)$$
$$- \left(\sum_{k=1}^{N} \psi_k \int_\Omega \frac{\partial \xi_k}{\partial x} \xi_i dxdy \right) \left(\sum_{k=1}^{N} \varphi_k \int_\Omega \frac{\partial \xi_k}{\partial y} \xi_i dxdy \right) + \frac{1}{\mathrm{Le}} \left[\sum_{k=1}^{N} \varphi_k \int_\Omega \left(\frac{\partial \xi_i}{\partial x} \frac{\partial \xi_k}{\partial x} + \frac{\partial \xi_i}{\partial y} \frac{\partial \xi_k}{\partial y} \right) \right] \quad (34)$$
$$+ \frac{Nt}{\mathrm{Le} \cdot Nb} \left[\sum_{k=1}^{N} \theta_{f_k} \int_\Omega \left(\frac{\partial \xi_i}{\partial x} \frac{\partial \xi_k}{\partial x} + \frac{\partial \xi_i}{\partial y} \frac{\partial \xi_k}{\partial y} \right) \right]$$

Using biquadratic functions with three-point Gaussian quadrature, the integrals in the residual equations are evaluated. Moreover, the nonlinear residual equations are solved utilizing the Newton–Raphson method to find out the coefficients of the expansions in Eq. (29). The detailed solution could be found in the previous studies (see Reddy, 1993; Basak et al., 2006a,b). Additionally, the computational domain comprises grid points in which the discretized equations were implemented. The nonuniform grid has been used in both x and y directions in which the grid points clustered near the walls. The iteration process terminates when the residuals for the stream functions become lower than 10^{-8}. Moreover, the time step ($\Delta\tau$) is adopted to be automatically adjustable. The present model, in the form of an in-house computational fluid dynamics (CFD) code, has been validated successfully against the work conducted by Saeid and Pop (2004) for unsteady free convection in a square cavity filled with a porous medium.

Based on the previous studies, the Lewis number is large in the order of 10^3 and greater, the magnitude of Nb and Nt are small in the order of 10^{-6}, and the buoyancy ratio parameter, the interface heat transfer parameters, and Nield numbers (Nhp and Nhs) are higher than unity (see Bhadauria and Agarwal, 2011). The modified thermal diffusivity ratio (ε_p) is about unity and higher, and the modified thermal capacity ratios (γ_p and γ_s) are of order 10.

To ensure an accurate solution that is independent of grid size, the average Nusselt number of three phases in the left hot wall, at $\tau = 0.5$, for different Rayleigh numbers and grid sizes is calculated (Table 1). It is depicted that the grid size of 100×100 provides precise results. Therefore the ensuing evaluations were conducted using the grid size of 100×100. It is worth mentioning that in this study, the evaluated Nusselt numbers are multiplied by the relevant nondimensional thermal conductivity coefficients.

Eliminating the effect of nanoparticles ($Nr = Nb = Nt = Nhp = 0$) and considering local thermal equilibrium, the present study reduces to the study of the transient free convection in a two-dimensional square cavity filled with a porous medium which was examined in the work represented by Saeid and Pop (2004). The variation of average Nusselt number as a function of nondimensional time (τ) for three different values of the Rayleigh number is computed by the CFD code and compared with the results presented by Saeid and Pop (2004). The results of the comparison are depicted in Fig. 2. Figure 2 shows that the average Nusselt numbers, computed in the present study, are in excellent agreement with the results reported in the literature.

4. RESULTS AND DISCUSSION

To evaluate the free convection of nanofluids in a porous cavity, the following typical values of the dimensionless parameters are adopted: Ra = 100, $Nr = 10$, $Nhs = Nhp = 10$, $\gamma_s = \gamma_p = 10$, $Nb = Nt = 10^{-6}$, and Le = 10^3.

TABLE 1: Grid independence test for Le = 1000, $Nb = Nt = 10^{-6}$, $\gamma_p = \gamma_s = 10$, $Nhp = Nhs = 10$, $\varepsilon = 0.5$, $\varepsilon_p = 1.0$, $\tau = 0.5$

	Ra = 100			**Ra = 1000**		
Grid size	$\overline{\mathbf{Nu}_s}$	$\overline{\mathbf{Nu}_f}$	$\overline{\mathbf{Nu}_p}$	$\overline{\mathbf{Nu}_s}$	$\overline{\mathbf{Nu}_f}$	$\overline{\mathbf{Nu}_p}$
50×50	1.3772	2.3512	3.4264	2.3852	10.048	11.985
70×70	1.3777	2.3509	3.4261	2.3888	10.038	11.972
100×100	1.3779	2.3507	3.4259	2.3911	10.031	11.965
120×120	1.3780	2.3507	3.4259	2.3921	10.029	11.963

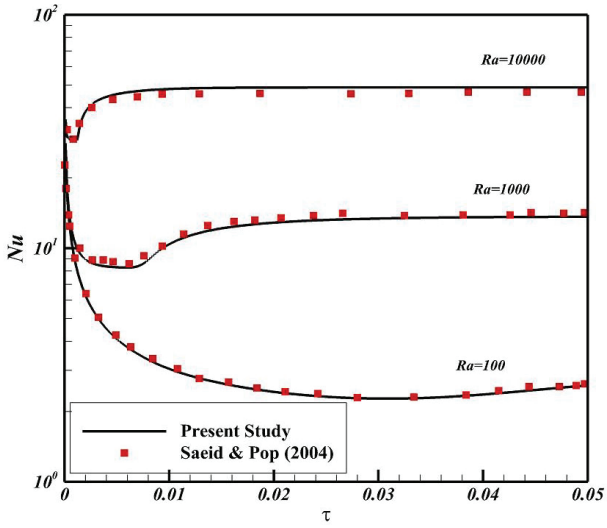

FIG. 2: Comparison of average Nusselt number with data adapted from Saeid and Pop (2004)

In the following calculations, the results are present for this set of nondimensional parameters unless in other cases the specified different parameters are mentioned. The isotherms of solid, fluid, and nanoparticles and streamlines for different times ranging from $\tau = 0.002$ to $\tau = 0.3$ are represented in Fig. 3. It is seen that early in the transient, the nanofluid adjacent to the hot wall moves up and falls downward near the cold wall, and also the isotherms are approximately parallel, which induces the conductive heat transfer in the core of the cavity. Furthermore, it is clear that the boundary layer for the solid phase is smaller than the fluid and nanoparticle ones. Studying the streamlines along with time, it could be seen that two large vortices are engendered near the two left hot and right cold walls in which the left recirculation is higher than the right one due to the flow direction of nanofluid. Shortly after that, these two vortexes become smaller and get close together to make a large recirculation about the middle of the enclosure. Finally, according to Fig. 3(h), the mentioned vortices disappear and merge together. On the other hand, as time goes on, the influence of convection on the isotherms becomes more obvious and stronger than conduction. As a result, the

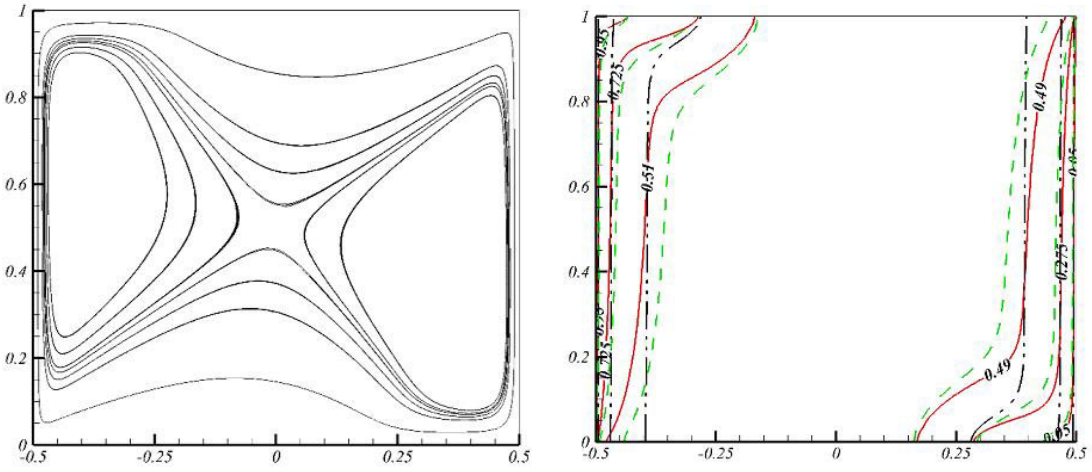

(a)

FIG. 3.

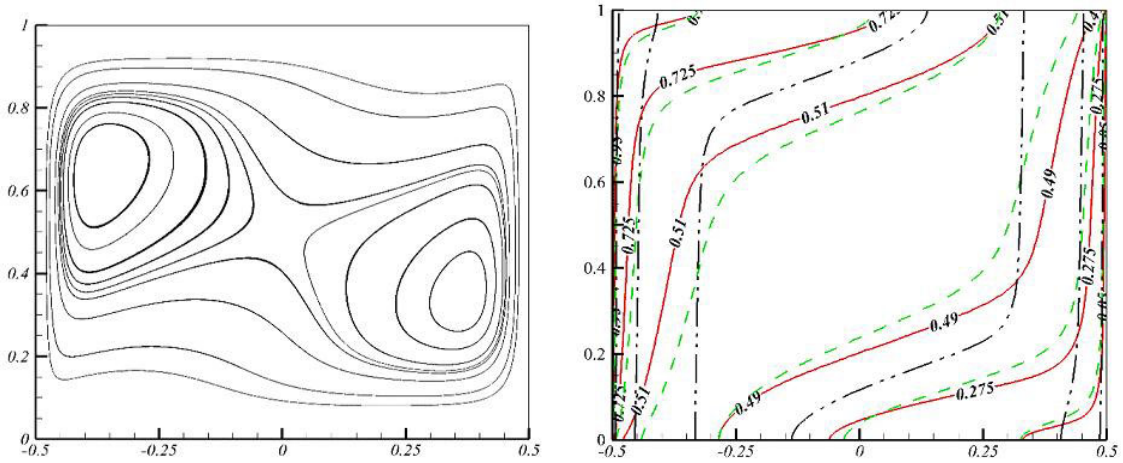

(b)

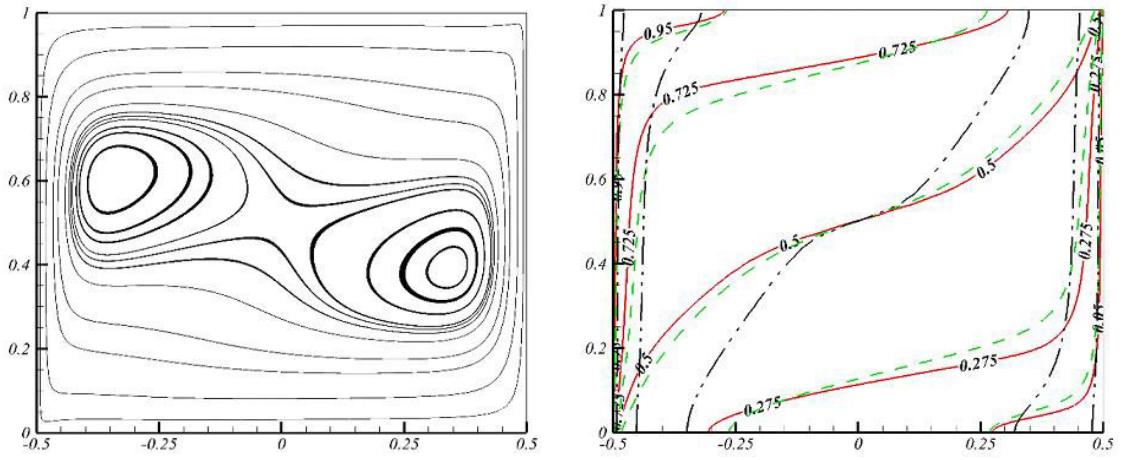

(c)

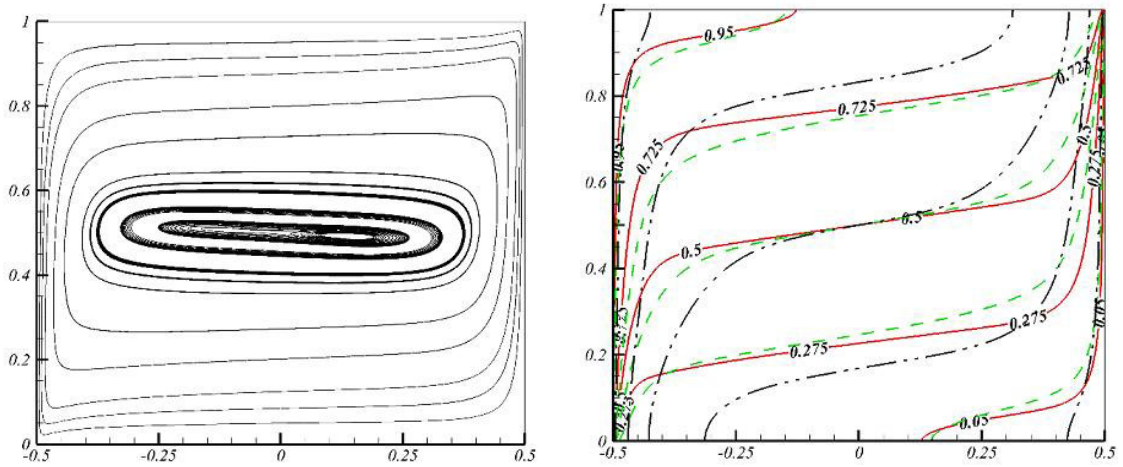

(d)

FIG. 3.

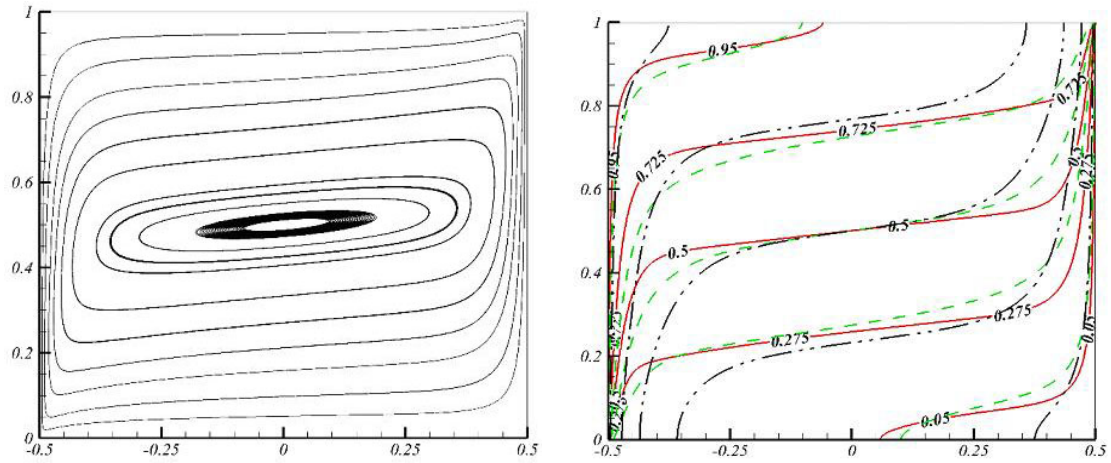

(e)

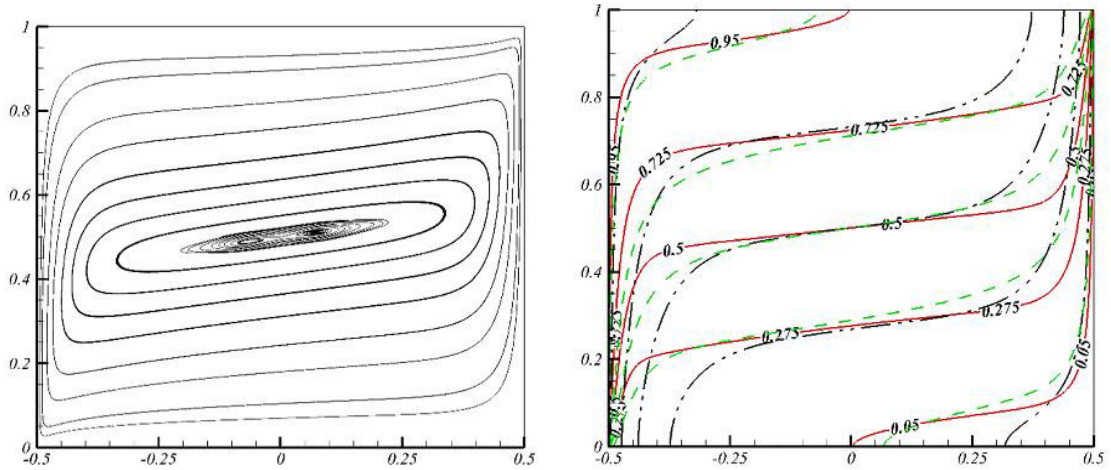

(f)

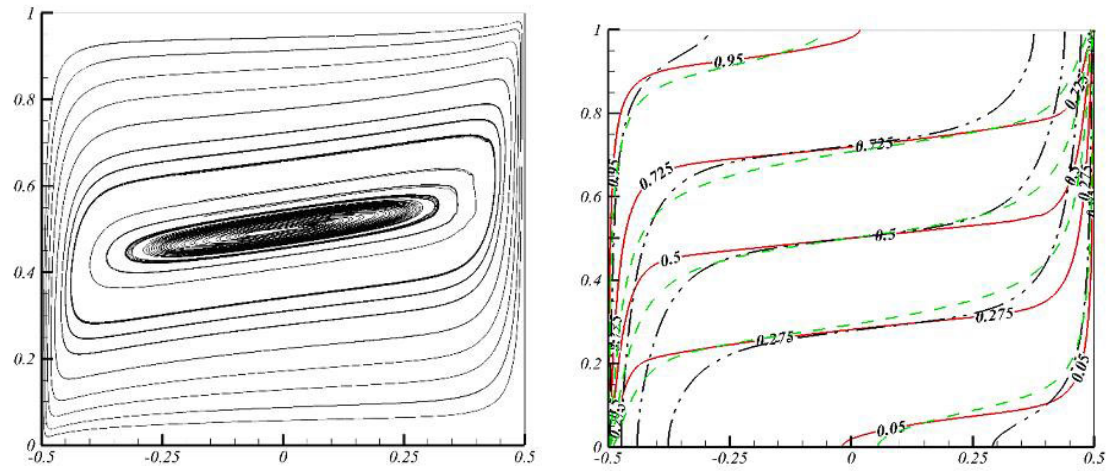

(g)

FIG. 3.

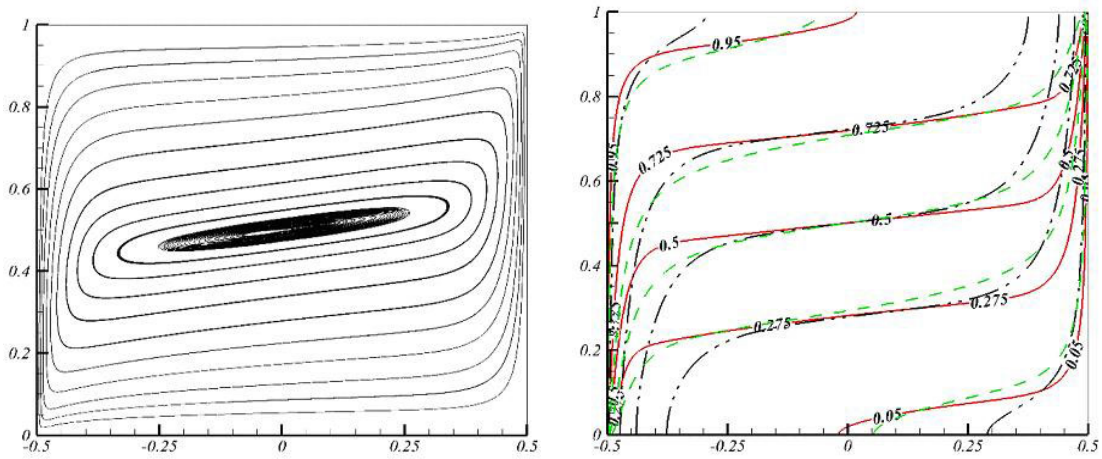

(h)

FIG. 3: (left) Streamlines and (right) isotherms in which solid, dashed, and dash-double-dotted lines indicate fluid, nanoparticles, and solid phases, respectively, for Ra $= 10^3$: (a) $\tau = 0.002$, (b) $\tau = 0.006$, (c) $\tau = 0.01$, (d) $\tau = 0.03$, (e) $\tau = 0.05$, (f) $\tau = 0.1$, (g) $\tau = 0.2$, (h) $\tau = 0.3$

solid, fluid, and nanoparticle boundary layers enlarge throughout the enclosure. In accordance with the isotherms and streamlines, for almost $\tau > 0.2$, the flow is going to attain a steady state regime. By comparing Fig. 3 for $\tau = 0.2$ and $\tau = 0.3$, it is clear that the streamlines and the isotherms are the same. It is worth mentioning that the concentration of nanoparticles undergoes a similar procedure as in Fig. 3, and hence it is not shown for the sake of brevity.

The nanofluid concentration is shown in Fig. 4 for $\tau = 0.5$. As it is seen, the concentration boundary layer is thin and the concentration of nanoparticles in the core of the enclosure is uniform because the Lewis number is high. In essence, the Lewis number is the ratio of thermal diffusivity of the nanofluid to the diffusion coefficient of nanoparticles in nanofluid. In fact, the thermal diffusivity is much larger than the nanoparticle diffusion coefficient; hence the Lewis number has a large magnitude. Moreover, in the theory of the boundary layer, the Lewis number indicates the relative proportion of the thickness of the thermal boundary layer to the thickness of the concentration

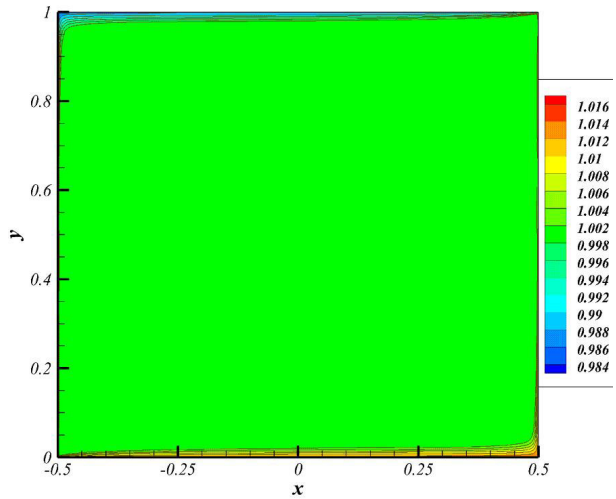

FIG. 4: The concentration of nanoparticles in nanofluid for $\tau = 0.5$

boundary layer. Since the thickness of the thermal boundary layer is mostly affected by the hydrodynamic boundary layer and the buoyancy forces, as the thickness of the thermal boundary layer is practically fixed, when the Lewis number is high, the concentration boundary layer is very thin.

The dependences of solid, fluid, and nanoparticle local Nusselt numbers on nondimensional time (τ) at the left hot wall have been represented in Fig. 5 for different positions of y. It could be seen that when the heating starts, instantly the value of Nu reaches infinity (in singular), and this is the characteristic of all the systems that are heated impulsively. In accordance with Fig. 5, it could be seen that in all phases, the value of the transient local Nusselt number for $y \geq 0.5$ decreases gradually and then is followed by a constant steady state magnitude. On the other hand, this value for $y < 0.5$ begins with a sharp decline in the early times and then goes up to reach to the steady Nusselt number. Figure 6 demonstrates the influence of γ_s and γ_p on the average Nusselt number along with dimensionless time.

Based on Fig. 6, it is clear that the variation of γ_p does not have any significant effect on the fluid and solid average Nusselt numbers. Conversely, the augmentation of γ_p increases the nanoparticle Nusselt number. Feasibly,

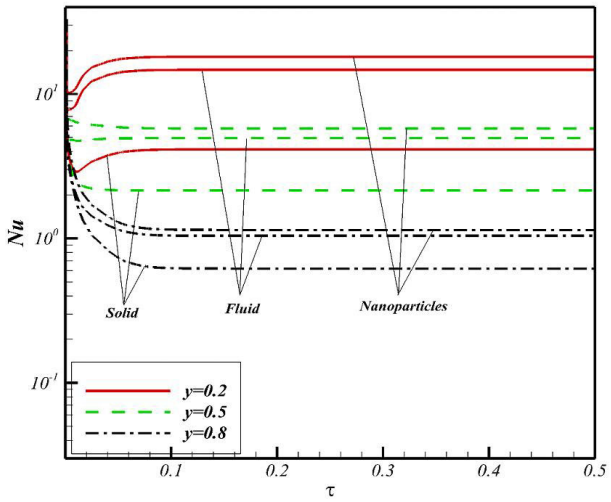

FIG. 5: Variation of transient local Nusselt number for different positions and Ra = 1000

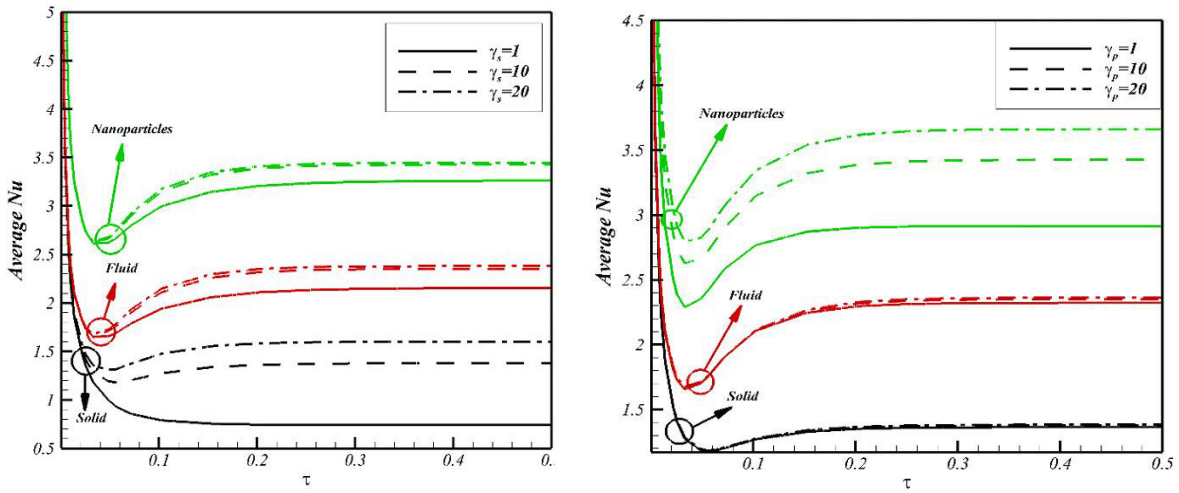

FIG. 6: Effect of variation of (left) γ_s and (right) γ_p on the average Nusselt number

any change in the parameter γ_p clearly affects the temperature of the nanoparticles directly [see Eq. (22)]. Moreover, the value of average Nusselt number for three phases falls down drastically and then gradually soars to its steady value in all γ_p magnitudes. On the other hand, it seems that apart from the solid Nusselt number, the variation of γ_s affects fluid and nanoparticle Nusselt numbers. Furthermore, it is glaringly obvious that the variation of γ_s and γ_p when these values are lower than 10 is more effectual than the case in which γ_s and γ_p are higher. In addition, an increase in γ_s causes a noticeable boost in average Nusselt number for three phases. Furthermore, the average Nusselt number of three phases has an increasing manner in solid, fluid, and nanoparticles, respectively. As a case in point, the value of average Nusselt number at $\gamma_s = 20$ for solid, fluid, and nanoparticles is 1.59, 2.38, and 3.44, respectively.

The influence of variation of Nhs on the solid, fluid, and nanoparticle transient average Nusselt number has been shown in Fig. 7. As substantiated in Fig. 7, though an increase in solid–fluid interface heat transfer parameter leads average Nusselt number of the solid to soar considerably, it causes a decrease in both nanoparticle and fluid average Nusselt numbers. Based on Eqs. (20)–(22), it could deduce that any change in Nhs has a direct impact on the solid and fluid temperatures. Moreover, in essence, the augmentation of Nhs intensifies the interaction between the fluid and solid matrix, and as a result, it tends to decline the temperature differences between two phases. It is notable that the alterations in temperature of nanoparticles are primarily the implication of interactions of base fluid and the nanoparticles. Therefore the temperature behaviors of nanoparticles and base fluid are the same for the most part.

The variation of average Nusselt number of solid, fluid, and nanoparticles for different Nhp has been depicted in Fig. 8. As expounded in Fig. 8, ascending the nanoparticle–fluid interface heat transfer parameter (Nhp) leads the average Nu of nanoparticles to notably increase. In contrast, the average Nusselt numbers of two other phases are poorly affected by Nhp variation. Additionally, it could be seen that when the nanoparticle–fluid interface heat transfer parameter has high value, the effect of fluctuation of this parameter on the average Nusselt number of three phases becomes less than the time in which Nhp is low.

The effect of buoyancy ratio parameter on the transient average Nusselt numbers has been illustrated in Fig. 9. According to Fig. 9, an increase of Nr causes the average Nusselt number to decrease for three phases. It is obvious that the mentioned marked decline in the base fluid and nanoparticles is more noticeable with respect to the porous solid matrix. In fact, the buoyancy ratio parameter is equivalent to the induced buoyancy mass transfer effects. It means that any increase of Nr leads to augmentation of the buoyancy mass transfer. For this reason, the augmentation of buoyancy ratio parameter would speed up the motion of the base fluid adjacent to the vertical wall, which results

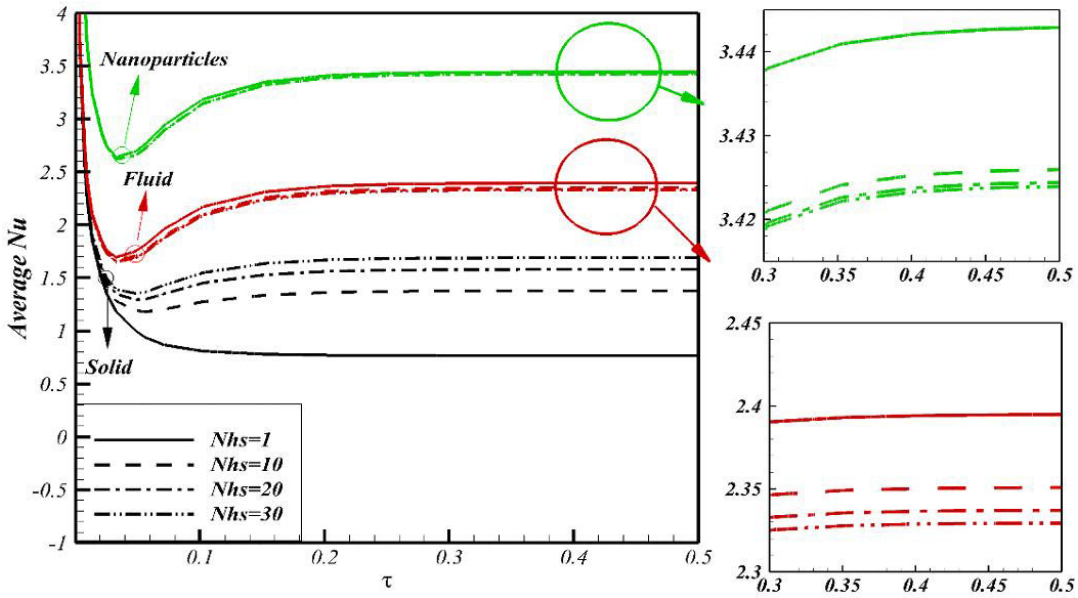

FIG. 7: Effect of Nhs on the average Nusselt numbers

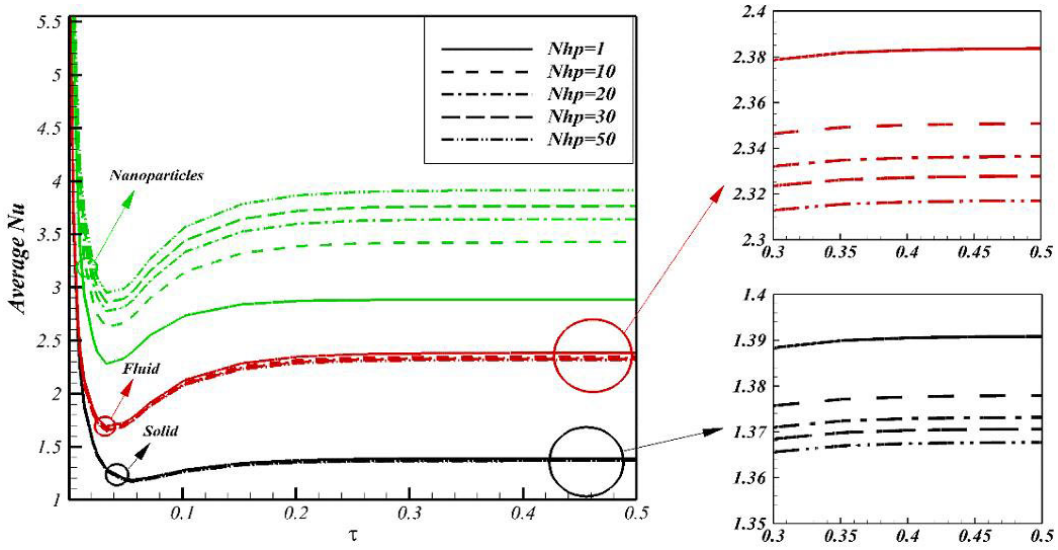

FIG. 8: Effect of Nhp on the average Nusselt numbers

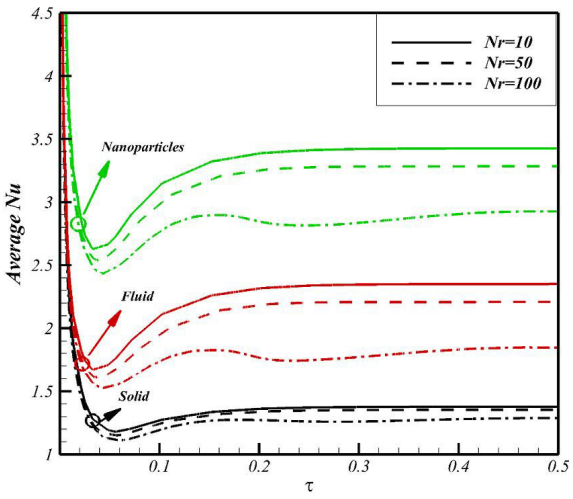

FIG. 9: Effect of Nr on the average Nusselt numbers

in the decrease in the temperature gradient (average Nusselt number). In addition, the fluctuation of the Nr induces direct conspicuous changes in the buoyancy forces in the vicinity of the vertical walls, which leads to resultant indirect variation of average Nusselt number (temperature gradient) of the base fluid. In consequence, the variation of the base fluid would influence the temperature gradient of the solid porous medium. Moreover, it seems that the increase of Nr would augment the time to reach steady state.

The eventual effect of Rayleigh number on the average Nusselt number of three phases is depicted in Fig. 10. It is illustrated that except for solid matrix, the behavior of variation of average Nusselt number is totally different at Ra $= 100$ in early times. In other words, the average Nu falls for Ra $= 100$, and then it follows by gradually increasing to reach its steady value. On the contrary, this value for base fluid and nanoparticles ascends drastically as time begins at Ra $= 1000$ and 10,000. Generally, it is clear that the augmentation of Ra tends to increase the average Nusselt number. Additionally, as Rayleigh number declines, the period of reaching steady state is increased.

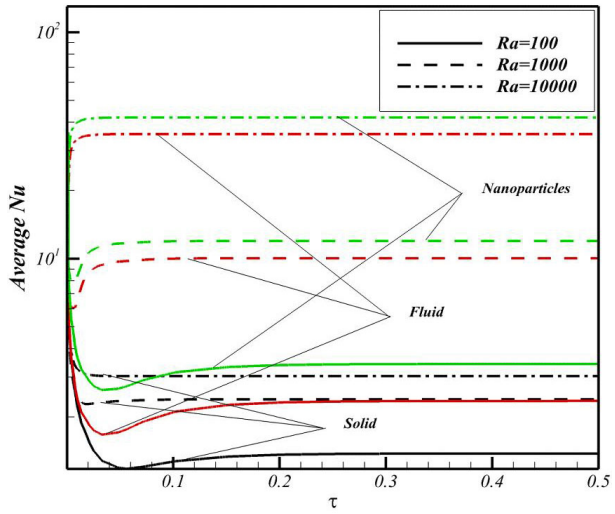

FIG. 10: Effect of Ra on the average Nusselt numbers

5. CONCLUSION

The transient natural convection in a porous enclosure saturated with a nanofluid is studied. Buongiorno's model for nanofluid and the local thermal nonequilibrium state for the mixture are adopted in the present study. Furthermore, it is considered that the motion of nanoparticles in the cavity is affected by Brownian and thermophoresis forces. The effect of thermophysical parameters on the Nusselt number is investigated. In a nutshell, the concentration boundary layer of the nanofluid is thin with respect to thermal ones. Moreover, the increase of γ_s and γ_p led to a substantial augmentation in the average Nusselt numbers of the solid matrix and nanoparticles, respectively. The decrease of Nr and increase of Ra would boost the average Nusselt number for all phases. Finally, the time to reach steady state is directly proportional to buoyancy ratio and reversely proportional to Rayleigh number.

ACKNOWLEDGMENTS

The second author acknowledges the financial support of Dezful Branch, Islamic Azad University, Dezful, Iran. The first and second authors acknowledge Iran Nanotechnology Initiative Council (INIC) for the financial support of the present study. The third author acknowledges the financial support of the Ministry of Education and Science of the Russian Federation (project 13.1919.2014/K). The first and second authors acknowledge the Sheikh Bahaei National High Performance Computing Center (SBNHPCC) for providing computational resources. SBNHPCC is supported by the Scientific and Technological Department of the Presidential Office and Isfahan University of Technology (IUT).

REFERENCES

Amiri, A. and Vafai, K., Analysis of dispersion effects and non-thermal equilibrium, non-Darcian, variable porosity incompressible flow through porous media, *Int. J. Heat Mass Transfer*, vol. **11**, pp. 939–954, 1994.

Amiri, A. and Vafai, K., Transient analysis of incompressible flow through a packed bed, *Int. J. Heat Mass Transfer*, vol. **41**, pp. 4259–4279, 1998.

Basak, T., Roy, S., and Balakrishnan, A.R., Effects of thermal boundary conditions on natural convection flows within a square cavity, *Int. J. Heat Mass Transfer*, vol. **49**, pp. 4525–4535, 2006a.

Basak, T., Roy, S., Paul, T., and Pop, I., Natural convection in a square cavity filled with a porous medium: Effects of various thermal boundary conditions, *Int. J. Heat Mass Transfer*, vol. **49**, pp. 1430–1441, 2006b.

Baytas, A.C., Thermal non-equilibrium natural convection in a square enclosure filled with a heat-generating solid phase, non-Darcy porous medium, *Int. J. Energy Res*., vol. **27**, pp. 975–988, 2003.

Baytas, A.C. and Pop, I., Free convection in a square porous cavity using a thermal non-equilibrium model, *Int. J. Thermal Sci*., vol. **41**, pp. 861–870, 2002.

Bejan, A., *Convection Heat Transfer*, 4th ed., New York, NY: John Wiley, 2013.

Bejan, A. and Kraus, A.D., Eds., *Heat Transfer Handbook*, New York, NY: John Wiley, 2003.

Bhadauria, B.S. and Agarwal, S., Convective transport in a nanofluid saturated porous layer with thermal non-equilibrium model, *Transp. Porous Media*, vol. **88**, pp. 107–131, 2011.

Buongiorno, J., Convective transport in nanofluids, *ASME J. Heat Transfer*, vol. **128**, pp. 240–250, 2006.

Choi, C., Yoo, H.S., and Oh, J.M., Preparation and heat transfer properties of nanoparticle-in-transformer oil dispersions as advanced energy-efficient coolants, *Current Appl. Phys.*, vol. **8**, pp. 710–712, 2008.

Gümgüm, S. and Tezer-Sezgin, M., DRBEM solution of mixed convection flow of nanofluids in enclosures with moving walls, *J. Comput. Appl. Math.*, vol. **259**, pp. 730–740, 2014.

Hirota, K., Sugimoto, M., Kato, M., Tsukagoshi, K., Tanigawa, T., and Sugimoto, H., Preparation of zinc oxide ceramics with a sustainable antibacterial activity under dark conditions, *Ceram. Int.*, vol. **36**, pp. 497–506, 2010.

Ingham, D.B. and Pop, I., Eds., *Transport Phenomena in Porous Media III*, Oxford, UK: Elsevier, 2005.

Jaballah, S., Sammouda, H., and Bennacer, R., Study of the mixed convection in a channel with porous layers using a thermal nonequilibrium model, *J. Porous Media*, vol. **15**, no. 1, pp. 51–62, 2012.

Jamalabadi, P.M.Y.A., Effects of micro- and macro-scale viscous dissipations with heat generation and local thermal non-equilibrium on thermal developing forced convection in saturated porous media, *J. Porous Media*, vol. **18**, no. 9, pp. 843–860, 2015.

Khanafer, K. and Vafai, K., A critical synthesis of thermophysical characteristics of nanofluids, *Int. J. Heat Mass Transfer*, vol. **54**, pp. 4410–4428, 2011.

Khashan, S.A., Al-Amiri, A.M., and Pop, I., Numerical simulation of natural convection heat transfer in a porous cavity heated from below using a non-Darcian and thermal non-equilibrium model, *Int. J. Heat Mass Transfer*, vol. **49**, pp. 1039–1049, 2006.

Kuznetsov, A.V. and Nield, D.A., Effect of local thermal non-equilibrium on the onset of convection in a porous medium layer saturated by a nanofluid, *Transp. Porous Media*, vol. **83**, pp. 425–436, 2010.

Kuznetsov, A.V. and Nield, D.A., The Cheng–Minkowycz problem for natural convective boundary layer flow in a porous medium saturated by a nanofluid: A revised model, *Int. J. Heat Mass Transfer*, vol. **65**, pp. 682–685, 2013.

Li, Y. and An, R., Two-level variational multiscale finite element methods for Navier–Stokes type variational inequality problem, *J. Comput. Appl. Math.*, vol. **290**, pp. 656–669, 2015.

Mahajan, A. and Sharma, M.K., Convection in magnetic nanofluids in porous media, *J. Porous Media*, vol. **17**, no. 5, pp. 439–455, 2014.

Muthtamilselvan, M., Transient buoyancy-driven convection of water saturated porous cavity near its density maximum, *Int. J. Comput. Methods Eng. Sci. Mech.*, vol. **12**, pp. 270–277, 2011.

Narasimhan, A., *Essentials of Heat and Fluid Flow in Porous Media*, Boca Raton, FL: CRC Press, 2013.

Nield, D.A. and Bejan, A., *Convection in Porous Media*, 4th ed., New York, NY: Springer, 2013.

Nield, D.A. and Kuznetsov, A.V., The Cheng–Minkowycz problem for natural convective boundary-layer flow in a porous medium saturated by a nanofluid, *Int. J. Heat Mass Transfer*, vol. **52**, pp. 5792–5795, 2009.

Nield, D.A. and Kuznetsov, A.V., Thermal instability in a porous medium layer saturated by a nanofluid: A revised model, *Int. J. Heat Mass Transfer*, vol. **68**, pp. 211–214, 2014.

Reddy, J.N., *An Introduction to the Finite Element Method*, New York, NY: McGraw-Hill, 1993.

Saeid, N.H. and Pop, I., Transient free convection in a square cavity filled with a porous medium, *Int. J. Heat Mass Transfer*, vol. **47**, pp. 1917–1924, 2004.

Schaefer, H.-E., *Nanoscience: The Science of the Small in Physics, Engineering, Chemistry, Biology and Medicine*, Berlin, Germany: Springer, 2009.

Shenoy, A., Sheremet, M., and Pop, I., *Convective Flow and Heat Transfer from Wavy Surfaces: Viscous Fluids, Porous Media and Nanofluids*, Boca Raton, FL: CRC Press, 2016.

Solin, P., Dubcova, L., and Kruis, J., Adaptive Hp-FEM with dynamical meshes for transient heat and moisture transfer problems, *J. Comput. Appl. Math.*, vol. **233**, pp. 3103–3112, 2010.

Srivastava, A.K., Bhadauria, B.S., and Kumar, J., Magnetoconvection in an anisotropic porous layer using thermal nonequilibrium model, *Spec. Topics Rev. Porous Media*, vol. **2**, no. 1, pp. 1–10, 2011.

Telionis, D.P., *Unsteady Viscous Flows*, New York, NY: Springer, 1981.

Tzou, D.Y., Instability of nanofluids in natural convection, *J. Heat Transfer*, vol. **130**, pp. 072401-1–072401-9, 2008a.

Tzou, D.Y., Thermal instability of nanofluids in natural convection, *Int. J. Heat Mass Transfer*, vol. **51**, pp. 2967–2979, 2008b.

Vadász, P., Ed., *Emerging Topics in Heat and Mass Transfer in Porous Media: From Bioengineering and Microelectronics to Nanotechnology*, vol. **22**, New York, NY: Springer, 2008.

Vafai, K., *Handbook of Porous Media*, 2nd ed., New York, NY: Taylor & Francis, 2005.

Vafai, K., *Porous Media: Application in Biological Systems and Biotechnology*, Boca Raton, FL: CRC Press, 2010.

Vafai, K. and Amiri, A., Thermal non-equilibrium forced convection in porous media, in *Transport Phenomena in Porous Media*, D.B. Ingham and I. Pop, Eds., vol. **1**, Amsterdam, The Netherlands: Pergamon, pp. 313–329, 1998.

Wu, F. and Zhou, W., Local thermal nonequilibrium effects on natural convection in a porous cavity heated and cooled from the side in a spatially sinusoidal manner, *J. Porous Media*, vol. **19**, no. 2, pp. 113–129, 2016.

Zhang, L., Ding, Y., Povey, M., and York, D., ZnO nanofluids—A potential antibacterial agent, *Progr. Nat. Sci.*, vol. **18**, pp. 939–944, 2008.